

Design and Optimization of PID Controller using Various Algorithms for Micro-Robotics System

Ehab Seif Ghith ^{1,*}, Farid Abdel Aziz Tolba ²

^{1,2}Department of Mechatronics, Faculty of Engineering, Ain shams University.

Email: ¹drehabghih1978@gmail.com, ²farid_tolba@eng.asu.edu.eg

* Corresponding Author

Abstract— Microparticles have the potentials to be used for many medical purposes in-side the human body such as drug delivery and other operations. This paper attempts to provide a thorough comparison between five meta-heuristic search algorithms: Sparrow Search Algorithm (SSA), Flower Pollination Algorithm (FPA), Slime Mould Algorithm (SMA), Marine Predator Algorithm (MPA), and Multi-Verse Optimizer (MVO). These approaches were used to calculate the PID controller optimal indicators with the application of different functions, including Integral Absolute Error (IAE), Integral of Time Multiplied by Square Error (ITSE), Integral Square Time multiplied square Error (ISTES), Integral Square Error (ISE), Integral of Square Time multiplied by square Error (ISTSE), and Integral of Time multiplied by Absolute Error (ITAE). Every method of controlling was presented in a MATLAB Simulink numerical model, and LABVIEW software was used to run the experimental tests. It is observed that the MPA technique achieves the highest values of settling error for both simulation and experimental results among other control approaches, while the SSA approach reduces the settling error by 50% compared to former experiments. The results indicate that SSA is the best method among all approaches and that ISTES is the best choice of PID for optimizing the controlling parameters.

Keywords—Sparrow Search Algorithm; Flower Pollination Algorithm; Slime Mould Algorithm; Marine Predator Algorithm; Multi-Verse Optimizer; Minimally invasive surgery; PID controller.

I. INTRODUCTION

For minimizing the trauma of surgical patients, Minimal Invasive Surgery (MIS) is recommended because it provides clinicians the comfort to go deep in every site of the human body. Along with that, thanks to the minimal invasive surgery, patients are required to spend less time in hospitals. Hence, it is also a cost-effective option. Laparoscopy is one of such surgeries which are implemented these days [1]. The instruments used in this process are usually small, and the operation is conducted by observing the images taken through the instrumental camera. Different variances of the two surgical methods are exhibited in Fig. 1.

Robots are used for reducing the invasiveness of minimal invasive surgery. They help in providing treatment to patients for whom surgeries are not recommended. Robotics is used to guide the accurate site for needle insertion in the body. Similarly, these robots are of great use in achieving the target required for the drug delivery, diagnosis, and treatment. In case of a smaller robot, the penetration depth inside the body

is elevated leading to effective pathways of medicinal travel in the body.

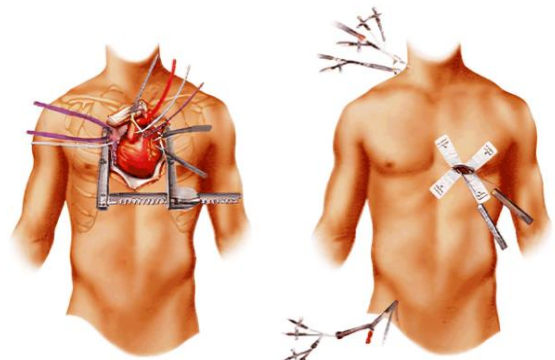


Fig. 1. Image on the left exhibits an orthodox open heart surgery, whereas image on the right depicts minimal invasive surgery of heart such as laparoscopy [1].

For the spherical site, Jasper D. et al. [2] have effectively constructed paramagnetic micro particles, which have a settling error of 8.4 μm when the system arrives at the control position. The average diameter of these micro-particles was 100 μm and a hollow coil was used in the experiment. The same experiment was conducted by Ramy et al. [3] by using a solid coil, and the settling error in this experiment was 8 μm . In the present study, the same experiment was conducted and the settling error achieved was 4 μm . It was observed that the SSA approach reduced the error rate up to 50% when compared with the previous experiments.

In order to achieve control goals, a sufficient and suitable design of the controller is necessary. Although different control methods have been developed, PID is still used because of being tunable, easily implemented, and quite simple in structure [4]-[10]. However, properly tuning the PID controller in such a way to become optimally efficient is still not easy. Among the different designs suggested, one of the best known methods of PID control is Ziegler and Nichols. However, achieving the greatest performance by this method can be challenging. Moreover, according to the usual method, tuning requires extra complex mathematical calculations [11], [12]. To avoid such different tuning, methods and artificial intelligence-based methods of optimization are preferred.

In different fields of engineering, multiple optimization techniques are used for supporting the meta-heuristic algorithms. These techniques do not require any kind of gradient information or flexibility, and their implementation

is also comparatively easy. Meta-heuristic techniques include either single-based or population-based algorithms. Single-based algorithm or trajectory algorithm is the optimization algorithm in which a single optimal solution is generated, whereas other algorithms, i.e., population-based, is capable of generating multiple solutions often redundant in nature. Five major types of algorithms can be named: Human, chemical, swarm intelligence, physics, and evolutionary-based optimization algorithm [13]-[33].

The current study presents our contribution which addresses two main parts:

- (i) A comparative study of six different functions: ISTSE, ITSE, ISE, ISTES, ITAE, and IAE during processing to achieve the parameters of control. The better performance of the above functions will be used to compare the dynamic characteristics of different control techniques.
- (ii) A comparative study of five novel optimization techniques; FPA, SSA, SMA, MPA, and MVO are conducted. The former techniques have been discussed for having good outcomes required to tune a controller of PID according to their settling, rising time and settling error. The tuning of PID controller is performed by minimizing the role obtained by fitness integral time square multiplied by error square.

The current study also includes mathematical model of micro-robotics system, PID controller, fitness function types, optimization techniques, and the description system architecture in part II. In part III, the simulation, experimental results, and discussion are depicted, while part IV exhibits the future prospects and conclusion of this study. The data is collected by an experimental setup, of which some results are reported in [3] which is an extension of this work.

II. METHODS

A. Mathematical model

For designing particles, the paramagnetic material is used, and it is formed by iron-oxide in lactic acid. The diameter of these particles is $100\mu m$, and their velocity depends on two factors. The magnetic forces and viscous drag are induced by micro-particle which depends upon the magnetic field of coils. Moreover, maximum velocity is achieved if acceleration reaches zero and magnetic and viscous drag forces are equal. The following equation is used to define the magnetic force.

$$F = \nabla \alpha_p V_p B^2 \quad (1)$$

In this equation, the volume of particles is denoted by V_p , and the magnetic flux density is denoted by B . the magnetic flux density is dependent upon the time and distance, whereas V_p and α_p are the constants. V_p is further substituted by using the variables given below for force production, as represented in the equation given below.

$$F = \frac{4}{3} \pi \alpha_p r_p^3 \nabla B^2 \quad (2)$$

In the above-mentioned equation, the radius of micro-particles is denoted by r_p , whereas the following equation is used for drag force.

$$F_d = -6\pi\eta r_p v \quad (3)$$

Here, η represents viscosity, micro-particle's velocity is denoted by v with dependence upon the second law of motion provided by Newton.

$$\begin{aligned} \sum F &= m_p a_p \\ \frac{4}{3} \pi \alpha_p r_p^3 \nabla B^2 - 6\pi\eta r_p v &= m_p a_p \\ v &= \frac{\frac{4}{3} \pi \alpha_p r_p^3 \nabla B^2 - m_p a_p}{6\pi\eta r_p} \end{aligned} \quad (4)$$

In equation 4, micro-particles achieve a maximum velocity when particles' acceleration equals zero. By using the following equation, the maximum velocity is calculated as follows:

$$v_m = \frac{2}{9} \frac{\alpha_p r_p^2}{\eta} \nabla B^2 \quad (5)$$

The particles with spherical shape were considered perfect, and F_m was used to denote the stimulated utilizing force. The particle's speed with respect to liquid was associated with the drag force represented by F_d . If the liquid is found stable, particle's speed is associated with the drag. The following equation is used to designate a continuous time-model.

$$m\ddot{x} + C_d * \dot{x} = F_m \quad (6)$$

As observed by C_d , there is a continuous designation of drag *via the* drag Stokes of Reynolds which is low, \ddot{x} represents acceleration, \dot{x} represents velocity, and the particle mass is denoted by m . The transfer role of micro-particle is signified by using the following formula:

$$\frac{X(s)}{F_m(s)} = \frac{1}{ms^2 + C_d * s} \quad (7)$$

B. PID Controller

Among the major controller types, Ideal-PID is commonly used in the industry. The algorithm of PID controller is the most vastly used in this scope. It has the ability to improve the steady state and transient errors. When disturbances occur, the ideal PID loses its high performance. Feedback control loops normally use this algorithm as is or with minor variations [34]. These gains are proportional gain K_p , integral gain K_i , and derivative gain K_d . Every gain can act on the error which is usually achieved by subtracting a measured variable, i.e., the output from a set point that the user had inserted. Equation number 8 exhibits the PID controller's transfer function. The standard form of PID controller is illustrated in Fig. 2.

$$C_{PID}(s) = \frac{Y(s)}{E(s)} = K_p + \frac{K_i}{s} + K_d s \quad (8)$$

The basic structure of PID controller is depicted in Fig. 3. The main components of PID controller are optimization techniques, process, fitness function, and sensors.

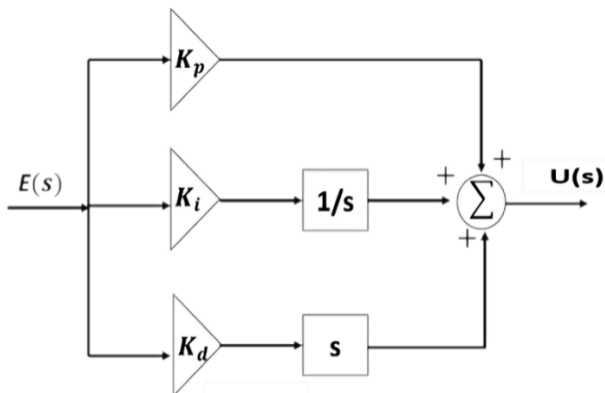


Fig. 2. Block diagram of the chief ideal PID controller.

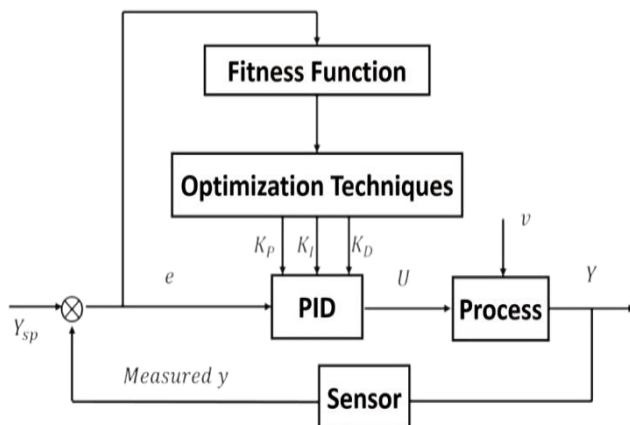


Fig. 3. Block diagram of PID controller

C. Fitness Functions Types

For designing any type of controllers, there are different optimum control parameters. Different parameters are computed to reduce the objective function. Due to the error of time-dependence, multiple functional objectives exist. The following equations define the different types of fitness functions [35]-[37].

Integral Absolute Error (IAE):

$$IAE = \int_0^{\infty} |e(t)| dt \quad (9)$$

Integral Square Error (ISE):

$$ISE = \int_0^{\infty} e^2(t) dt \quad (10)$$

Integral of Time multiplied Absolute Error (ITAE):

$$ITAE = \int_0^{\infty} t|e(t)| dt \quad (11)$$

Integral of Time multiplied square Error (ITSE):

$$ITSE = \int_0^{\infty} t e^2(t) dt \quad (12)$$

Integral Square Time multiplied square Error (ISTES):

$$ISTES = \int_0^{\infty} [t^2 e(t)]^2 dt \quad (13)$$

Integral of Square Time multiplied by square Error (ISTSE):

$$ISTSE = \int_0^{\infty} t^2 e^2(t) dt \quad (14)$$

The problem of optimization is formulated by using the following rules, i.e., objective function is minimized and subjected to:

$$K_{pmin} < K_p < K_{pmax}$$

$$K_{imin} < K_i < K_{imax}$$

$$K_{dmin} < K_d < K_{dmax}$$

D. Optimization Methods

Techniques of optimization have supported different meta-heuristic algorithms which have become popular within the engineering applications and fields. This is due to the need for flexibility for such trivial ideas which are easy in implementation and where gradient information is not required. Such techniques are required to pass the local optima and to be updated for tackling the wide problems that cover different disciplines and fields. These meta-heuristic and nature-inspired algorithms are capable of solving multiple problems of optimization which are used to represent the biological and physical phenomena.

Meta-heuristic techniques are mainly divided into two main algorithm categories: single-based and population-based algorithm. Single-based algorithm is capable of generating a single optimal solution on every run. It is also called trajectory algorithm, and it is enhanced when a neighboring methodology is used. The population-based algorithm generates multiple solutions on every run and is further classified into five types: Swarm intelligence, human, physical-, chemical, and evolutionary-based algorithms. In this evolutionary-based algorithm, the techniques use three main operations: Mutation, recombination, and selection. These techniques are inspired by nature's evolutionary phenomenon. For a swarm intelligent algorithm, the information is gathered on the basis of a collective behavior adopted by nature. Physical-based algorithm gathers information according to different theories obtained from the multiverse concept. Chemical-based algorithm uses chemical compounds and chemical rules for optimization, while humans and their actions are associated with human-based algorithm. Population-based algorithms have a standard feature in common as per their nature, and the search processes in such algorithms are categorized into two phases: Exploitation and exploration [38]-[54]. This meta-heuristic classification is presented in Fig. 4.

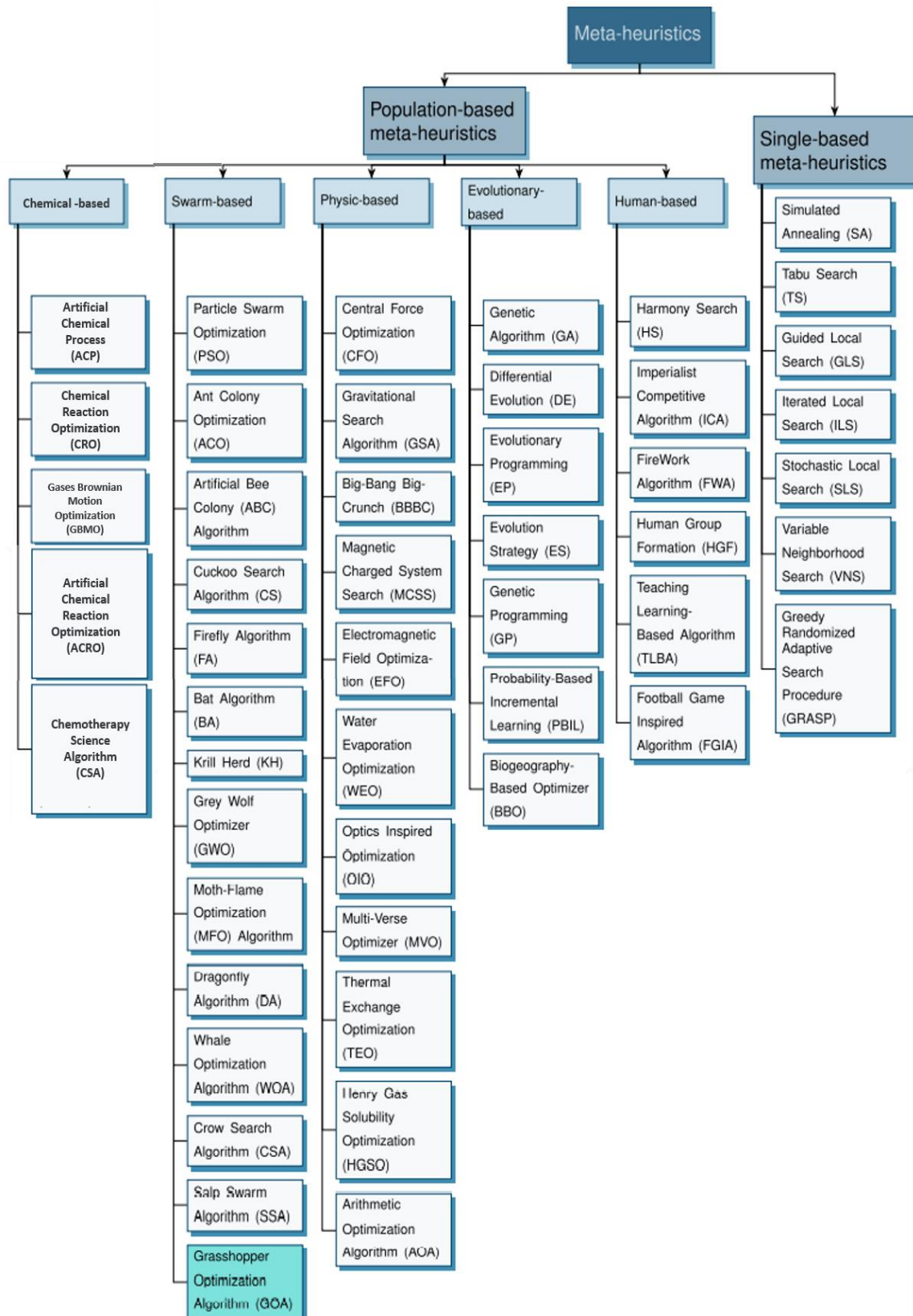


Fig. 4. Meta-heuristic optimization categorization methods [17].

- Sparrow Search Algorithm (SSA)

As described, SSA is a technique of swarm intelligence optimization. The main idea behind this algorithm was inspired by closely observing the sparrow population

behavior and the concept of foraging [55]. Depending on their behavioral characteristics, sparrows are classified into two groups: Producers and scroungers. Producers are the ones who have a larger space to locate the sources of food, and the other group which searches for food is called scroungers. The

formula of SSA is determined by using the following equations. The matrix given below is used to determine the position of sparrows.

$$X = \begin{bmatrix} X_{1,1} & \cdots & X_{1,d} \\ \vdots & \ddots & \vdots \\ X_{n,1} & \cdots & X_{n,d} \end{bmatrix} \quad (15)$$

In the equation presented above, d represents the total dimension numbers, and n is the total sparrow number. In case of high energy levels in sparrows, these are called producers. They are designated to find certain areas which have rich food supply and to scavenge such zones to scroungers. Sparrow's value of cost is evaluated by the formula given below.

$$F_x = \begin{bmatrix} f(X_{1,1}) & \cdots & f(X_{1,d}) \\ \vdots & \ddots & \vdots \\ f(X_{n,1}) & \cdots & f(X_{n,d}) \end{bmatrix} \quad (16)$$

Once sparrows locate the producers, alarming signals are produced for other sparrows depending upon the threshold criteria. Producers lead scroungers to a safe destination if the alarm value exceeds the safety threshold value. Producers which have the best cost value are more likely to find food than the scroungers. The following equation is used to update the position of producers continuously:

$$X_{i,j}^{t+1} = \begin{cases} X_{i,j}^t * \exp\left(-\frac{i}{\beta * iter_{max}}\right) & \text{if } R_2 < ST \\ X_{i,j}^t + Q * L & \text{if } R_2 \geq ST \end{cases} \quad (17)$$

In this equation, the producer's current position in j th dimension present in i th iteration is described by $X_{i,j}^t$, whereas the maximum number of iterations is denoted by $iter_{max}$. The threshold value is denoted by ST and falls in the range of $[0.5, 1]$, β denotes a random constant value ranging from $[0, 1]$, and the value of R_2 lies within $[0, 1]$. Hence, according to this equation, if the value of R_2 is lesser than the value of ST , there are zero predators, and producers can search for food sources globally. In other cases, R_2 is equal to or greater than ST . The equation used to update the position of scroungers is given below:

$$X_{i,j}^{t+1} \begin{cases} Q * \exp\left(\frac{X_{worst}^t - X_p^{t+1}}{i^2}\right) & \text{if } i > n/2 \\ X_p^{t+1} + |X_{i,j}^t - X_p^{t+1}| * A^+ * L & \text{Otherwise} \end{cases} \quad (18)$$

In this equation, A^+ is determined by $A^+ = A^T * (A * A^T)^{-1}$, X_p is the position value found by producer, and the value of the global worst population is represented by X_{worst} . These positions are determined according to the following equation:

$$X_{i,j}^{t+1} = \begin{cases} X_{best}^t + \alpha * |X_{i,j}^t - X_{best}^{t+1}| * x & \text{if } f_i > f_g \\ X_{i,j}^t + K * \left(\frac{|X_{i,j}^t - X_{worst}^{t+1}|}{(f_i - f_\omega) + \varepsilon}\right) & \text{if } f_i = f_g \end{cases} \quad (19)$$

In this equation, X_{best}^t is the value of the current global optimal location, K is a random value, α is another random

value which is normally distributed with a variance of 1 and a mean value of 0, f_ω is the worst fitness value, and f_i and f_g are the current individual and global best costs respectively. The flowchart is present in Fig. 5.

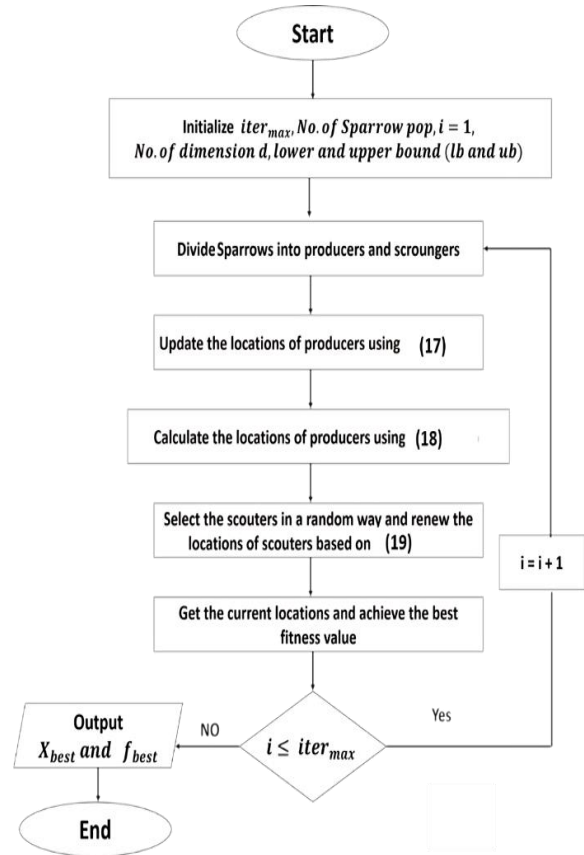


Fig. 5. Flowchart of the SSA [55]

• Flower Pollination Algorithm (FPA) Optimization

This algorithm was proposed by Xin-She Yany in 2012. This optimization algorithm acts like the pollination behavior of a flowering plant [56]. Pollinators include butterflies, bats, insects, and birds. Pollination in general is of two types. The first type is biotic in which birds and insects are involved, and it is noted that 90% pollination is biotic. The second type is abiotic in which no pollinators of any external source are involved. Pollination is also classified into cross and self-pollination which are presented in Fig. 6.

Cross-pollination occurs when pollens are transferred from one flower to another. If pollination occurs within the same flower, it is called self-pollination which doesn't require any external pollinator. If pollination occurs between flowers present at long distances apart, it is defined as global pollination. For global pollination, the pollinator has to jump a few steps and follow the function of levy distribution. The feature is described according to the equations (20 – 23).

$$X_i^{t+1} = X_i^t + L(X_i^t - g^*) \quad (20)$$

$$X_i^{t+1} = X_i^t + \varepsilon(X_i^t - X_k^t) \quad (21)$$

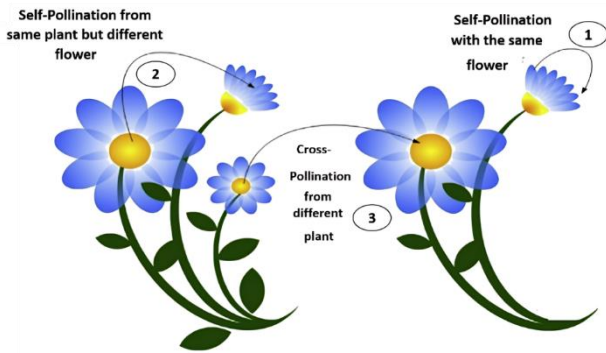


Fig. 6. Flower pollination occurring in different forms [56]

In the above-mentioned equation, the desired result vector is given by X_i^t , the current best solution is represented by g^* , step size according to levy distribution is given by L , whereas a random variable which follows the normal distribution is represented by ε . The following equation represents the levy steps in global pollination.

$$L = \frac{1}{S^{1+\beta}} \tag{22}$$

Here, levy function exponent is denoted by β , while S is calculated by the equation given below:

$$S = \frac{u}{|v|^{1+\beta}} \tag{23}$$

In this equation, $u \sim N(0,1)$, and $v \sim N(0, \sigma^2)$, in which σ is the value of standard deviation based on normal distribution. Fig. 7 describes FPA's flowchart.

• **Slime Mould Algorithm (SMA)**

Slime Mould Algorithm (SMA) is one of the metaheuristic methods of optimization which is recently developed and depends upon NFL It has exhibited success and improvement in solving different problems associated with engineering. This algorithm uses the representation of Physarum Polycephalum model behavior, and the mathematical operation is divided into three major phases [57].

Approaching Food: To approach food, the smell present in air is used to attract the slime mould towards food. The following equation is used to describe this behavior:

$$\overrightarrow{X}(t+1) = \begin{cases} \overrightarrow{X}_b(t) + \overrightarrow{vb}.(\overrightarrow{W}. \overrightarrow{X}_A(t) - \overrightarrow{X}_B(t)), & r < p \\ \overrightarrow{vc}.\overrightarrow{X}(t), & r \geq p \end{cases} \tag{24}$$

Slime mould location is represented by \overrightarrow{X} , and the location where the order is present in highest concentration is denoted by \overrightarrow{X}_b . The population selected randomly from the slime mould is denoted by \overrightarrow{X}_A and \overrightarrow{X}_B . The value of \overrightarrow{vb} ranges from $[-a, a]$, and the following formula is used to define the value of a :

$$a = \operatorname{arctanh}\left(-\left(\frac{t}{t_{max}}\right) + 1\right) \tag{25}$$

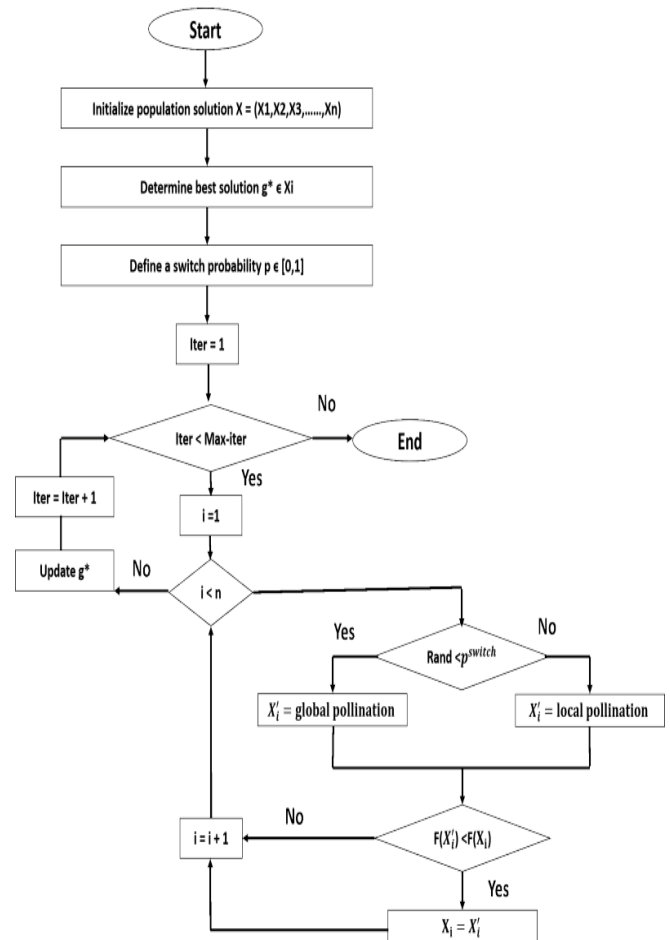


Fig. 7. Flow-chart of the solutions of FPA [56].

In the above-mentioned equation, the current iteration is denoted by t and the maximum iterations number is expressed as t_{max} , whereas \overrightarrow{vc} is the parameter reduced from 1 to 0, and p is expressed as follows:

$$p = \tanh |S(i) - DF| \tag{26}$$

In this equation, $i \in 1,2,3, \dots, n$, the function of fitness of \overrightarrow{X} is determined by $S(i)$, whereas during different algorithm iterations, DF represents the best fitness function. Slime mould weight is defined by \overrightarrow{W} and described according to the following equation:

$$\overrightarrow{W}(\operatorname{Smellindex}(i)) = \begin{cases} 1 + r. \log\left(\frac{bf - S(i)}{bF - wF}\right) + 1, & \text{condition} \\ 1 - r. \log\left(\frac{bf - S(i)}{bF - wF}\right) + 1, & \text{others} \end{cases} \tag{27}$$

$$\operatorname{Smellindex} = \operatorname{sort}(S) \tag{28}$$

In the above-mentioned equation, $S(i)$ indicates the population first half. $[0, 1]$ is the range of a random value denoted by r , the function in current iteration of optimal fitness and worst fitness is denoted by bF , and the optimal fitness function in current iteration is denoted by wf . Sorting is carried out in ascending order to search for the location of

individual \vec{X} , and is updated according to the best location \vec{X}_b as presented in Fig. 8.

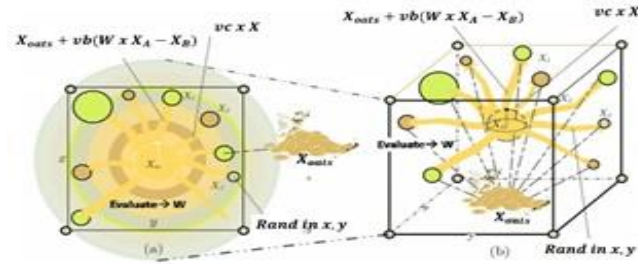


Fig. 8. Site of Slime Mould with dimensions 2D and 3D [57].

Wrapping Food: The second phase in optimizing SMA is wrapping food in which a mathematical form is used to improve the slime mould. Whenever food is available in a maximum concentration, slime mould produces a strong wave in the vein which leads to a rapid flow of cytoplasm. Equation 29 represents the relationship between concentration of food and veins' width. For the assessment of the relationship between food concentration and veins, it is concluded that in the regions in which food is more concentrated, the weight of veins is high, while in regions where food is less concentrated, the weight of veins is low leading to the exploration of other regions depending on the identification of food concentrations. The updated location is evaluated according to the equation given below:

$$\vec{X}^* = \begin{cases} rand.(UB - LB) + LB, rand < z \\ \vec{X}_b(t) + vb.(W.X_A(t) - X_B(t)), r < p \\ \vec{vc}.X(t), r \geq p \end{cases} \quad (29)$$

In this equation, LB and UB are the lower and upper bounds present in search spaces, while z is the value between the range of $[0, 0.1]$, and r and $rand$ are the values within $[0, 1]$.

Oscillations: Propagation of waves that originated due to biological changes occurring inside the veins is the idea on which slime mould operates. This is why it is important to find a location where intensified food concentration is present. These variations are modelled by three main parameters which are used for simulation update and include \vec{vc} , \vec{vb} and W . The flowchart of slime mould algorithm is given in Fig. 9.

• **Marine Predator Algorithm (MPA)**

This technique depends on the forging behavior of predators that are ocean dwellers. To capture their prey, they use two main strategies: Levy motion and Brownian motion. Levy relies mostly on small steps and long leaps, whereas the second technique uses Brownian movement to identify regular and recognised steps. There are three phases of MPA, i.e., initialization, elite, and prey and optimization, which are depicted below in detail [58], [59].

Initialization Stage: In this phase, solutions are distributed in a uniform manner and can be expressed by using the following equation:

$$\vec{P} = \vec{P}_L + r(\vec{P}_u - \vec{P}_L) \quad (30)$$

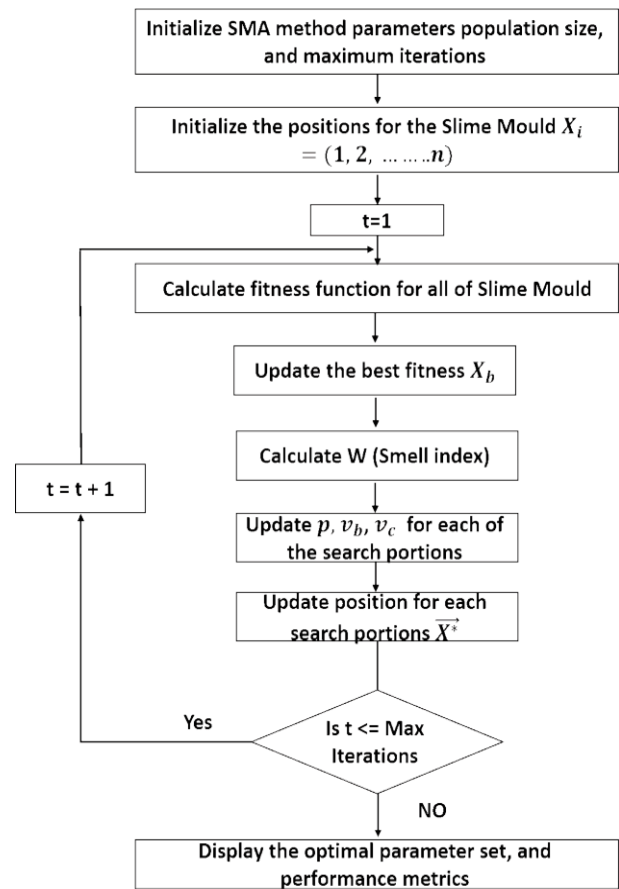


Fig. 9. Solution procedures flowchart of Slime Mould Algorithm [57].

Here, the lower and higher constraint vector of problem variables is denoted by \vec{P}_u and \vec{P}_L , and r is the value distributed randomly in the range of 0-1.

Elite and prey matrix development: This depends on the predator that wants to survive the longest, which is why most fit predators are selected to develop a matrix defined by elite matrix (EM) to involve the best fittest solution. This matrix is given by the following equation:

$$EM = \begin{bmatrix} P_{1,1}^f & P_{1,2}^f & \dots & P_{1,d}^f \\ P_{2,1}^f & P_{2,1}^f & \dots & P_{2,d}^f \\ \vdots & \vdots & \vdots & \vdots \\ P_{n,1}^f & P_{n,2}^f & \dots & P_{n,d}^f \end{bmatrix} \quad (31)$$

EM defines the set of n rows which suggests the agent's number, and d represents the dimension number. Most fit predictor vectors are denoted by P^f , and this matrix is updated at every iteration till the end and predicts another predator.

Prey matrix (PM) is another matrix that is designed to search for its own food. EM and PM both have an equal number of columns or rows. Here, the predator updates its position and current location according to the prey's position. This can be expressed according to the following equation:

$$PM = \begin{bmatrix} P_{1,1}^f & P_{1,2}^f & \dots & P_{1,d}^f \\ P_{2,1}^f & P_{2,2}^f & \dots & P_{2,d}^f \\ \vdots & \vdots & \vdots & \vdots \\ P_{n,1}^f & P_{n,2}^f & \dots & P_{n,d}^f \end{bmatrix} \quad (32)$$

Optimization Algorithm: This algorithm is divided into three sub-phases according to the prey velocity ration which is quite relevant to the predator. These sub-phases are described below.

High VR Sub-Phase: In this sub-phase, an exploration phase is expressed. If VR is greater than 10, the Brownian motion is applied by the prey to help in searching for the food for having an efficient domain exploration. In the case of high VR, the predator looks for prey even if it doesn't make any motion. VR is defined by the following equations:

$$\text{While } t < \frac{t_{max}}{3} \quad (32)$$

$$\overrightarrow{SS}_i = \overrightarrow{R}_B \otimes (\overrightarrow{EM}_i - \overrightarrow{R}_B \otimes \overrightarrow{PM}_i) \quad (33)$$

$$\overrightarrow{PM}_i = \overrightarrow{PM}_i + P * \overrightarrow{R} \otimes \overrightarrow{SS}_i \quad (34)$$

In the above-mentioned equation, i is a search agent, the movement of its step size is denoted by \overrightarrow{SS}_i , whereas \overrightarrow{R}_B is a vector which is the collection of multiple values taken at random and defined as Brownian. In the equation, \otimes denotes element multiplication, while a constant number whose value is 0.5 is denoted by P , similarly t_{max} and t represent the total number of iterations and current number of iterations, respectively and \overrightarrow{R} is the value which consists of a number taken at random.

Unity VR Sub-Phase: The unity phase represents a mixed result of exploitation and exploration and is divided into two major halves. In this phase, the predator uses the Brownian movement to have a better exploration, whereas the prey uses levy flights for the improvement of better exploitation. The following equation is used to represent this phase.

$$\text{While } \frac{t_{max}}{3} < t < \frac{2t_{max}}{3}$$

The following equation represents the first half of search agents:

$$\overrightarrow{SS}_i = \overrightarrow{R}_i \otimes (\overrightarrow{EM}_i - \overrightarrow{R}_i \otimes \overrightarrow{PM}_i) \quad (35)$$

$$\overrightarrow{PM}_i = \overrightarrow{PM}_i \otimes P * \overrightarrow{R} \otimes \overrightarrow{SS}_i \quad (36)$$

To evaluate the second half, the following equation is used:

$$\overrightarrow{SS}_i = \overrightarrow{R}_B \otimes (\overrightarrow{R}_B \otimes \overrightarrow{EM}_i - \overrightarrow{PM}_i) \quad (37)$$

$$\overrightarrow{PM}_i = \overrightarrow{EM}_i + P * CF \otimes \overrightarrow{SS}_i \quad (38)$$

$$CF = \left(1 - \frac{t}{t_{max}}\right)^{2t} \quad (39)$$

In the above-mentioned equation, a vector having values distributed randomly and manifesting levy flights is denoted by \overrightarrow{R}_L . There is also a known variable used to intensify the motion of predator by step-size improvement and is denoted by CF .

Low VR Sub-phase: A sub-phase involving the exploitation strategy which uses levy flight on predators for improvement is represented by the following equations:

$$\text{While } > \frac{2 * t_{max}}{3}$$

$$\overrightarrow{SS}_i = \overrightarrow{R}_i \otimes (\overrightarrow{R}_L - \overrightarrow{R}_L \otimes \overrightarrow{EM}_i - \overrightarrow{PM}_i) \quad (40)$$

$$\overrightarrow{PM}_i = \overrightarrow{EM}_i + P * CF \otimes \overrightarrow{SS}_i \quad (41)$$

Fish Aggregating Devices (FADs): It is a fact that the lives of the predators in their surrounding environment have a very heavy influence on their foraging behaviour. Out of many external issues, FDA's major issue is that it must help MPA in staying away from dropping down into the local optima. This influence is represented according to the following formula.

$$\begin{aligned} \overrightarrow{PM}_i &= \begin{cases} \overrightarrow{PM}_i + CF [\overrightarrow{P}_i + \overrightarrow{R} \otimes (\overrightarrow{P}_u - \overrightarrow{P}_L)] \otimes \overrightarrow{U} & \text{if } r < \text{FADS} \\ \overrightarrow{PM}_i + [\text{FADS} (1 - r) + r](\overrightarrow{PM}_{r1} - \overrightarrow{PM}_{r2}) & \text{if } r \geq \text{FADS} \end{cases} \\ & \quad (42) \end{aligned}$$

In this equation, r is a value taken at random by falling in the local solutions of optima and ranges from [0, 1], FADs are set to a value equal to 0.2, $r1$ and $r2$ are the random indices obtained by the prey matrix, and \overrightarrow{U} is the value of a vector consisting of either 0 or 1.

Marine Memory: Marine memory is the final stage related to the estimation of fitness value during every iteration of the positions already saved. In this phase, the current and saved locations are exchanged to obtain the best value of fitness. Fig. 10. exhibits the flowchart of MPA

• Multi-Verse Optimization Algorithm (MVO)

One of the population-based algorithms is multi-verse optimization (MVO) proposed by Mirjalili et al. [60]. The inspiration for this optimization technique relies on some concepts in the science of cosmology, such as white-hole, black-hole, and warm hole. The main aim of such concepts is achievement of the exploration and exploitation phases. This algorithm's mathematical model is built on a crucial concept wherein the universe is comparable to a solution. Furthermore, each person in the population is seen to represent a solution for a certain item in the cosmos. The population is formed based on a set of the universe defined using the following equation:

$$M = \begin{bmatrix} X_1^1 & X_1^2 & \dots & X_1^d \\ X_2^1 & X_2^2 & \dots & X_2^d \\ \vdots & \vdots & \vdots & \vdots \\ X_n^1 & X_n^2 & \dots & X_n^d \end{bmatrix} \quad (43)$$

Based on equation (43), it can be seen that d and n are known as the number of variables and universe, respectively. The representation of the j th parameter of the i th universe X_i^j can be defined using the following equation:

$$X_i^j = \begin{cases} X_k^j & r1 < NI(U_i) \\ X_i^j & r2 \geq NI(U_i) \end{cases} \quad (44)$$

Where U_i is known as the i th universe, $NI(U_i)$ is known as the normalized inflation rate, X_i^j is the j th parameter of the k th universe, and $r1$ is considered a random number within the range $[0, 1]$.

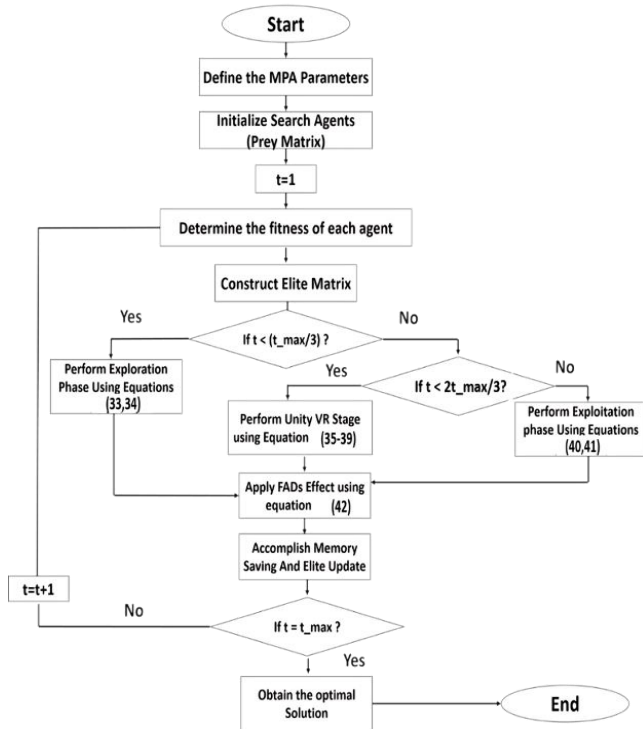


Fig. 10. MPA flowchart [59].

To carry out the exploitation process, it may be assumed that each universe contains separate wormholes that are utilized to move items across space in a random manner without taking the inflation rate into account. To improve the inflation rate and provide local variances for each universe, the worm holes are demonstrated in terms of optimal universes reached so far. The demonstration of the former method can be expressed in the following equation:

$$X_i^j = \begin{cases} X_j^j & r2 \geq WEP \\ X_j - TDR \times ((ub_j - lb_j) \times r_4 + lb_j) & r3 \geq 0.5, r2 < WEP \\ X_j - TDR \times ((ub_j - lb_j) \times r_4 + lb_j) & r3 \geq 0.5, r2 > WEP \end{cases} \quad (45)$$

Where X_j represents the j th parameter of the best universe obtained, lb_j and ub_j are the minimum and maximum bounds of the j th variable, X_i^j is the j th parameter of the i th universe, and $r2$, $r3$, and $r4$ are the random numbers within the range $[0, 1]$.

Here, WEP and TDR are the wormhole existence and the travelling distance rate coefficients probability, respectively. For using these parameters, the linearity concept is increased over iteration in order to include the exploitation stage. TDR explains the variation as the rate of distance for the object moving in wormhole to be optimum and the best universe to be enhanced. During iterations, WEP and TDR are raised for achieving the local search and effective exploitation around the universe obtained optimally. WEP and TDR are represented by the equations given below:

$$WEP = \min + l \times \left(\frac{\max - \min}{L} \right) \quad (46)$$

$$TDR = 1 - \frac{1}{L^p} \quad (47)$$

E. System Architecture

There are seven components of system architecture: Coils, control algorithms, reservoir, real time controllers, power supply units, microscope cameras, and pantograph robots. Fig. 11 displays the major components of micro-particle in 2D space.

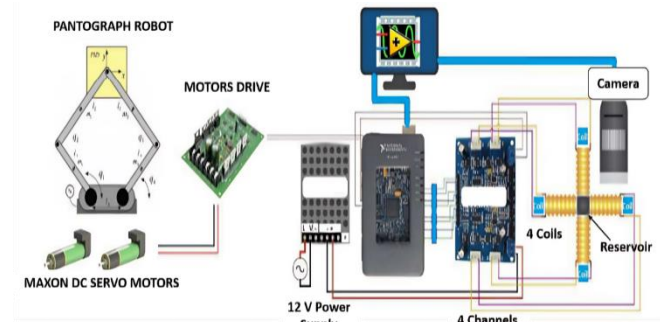


Fig. 11. Micro-particle's complete system architecture in 2D space [3]

III. RESULTS AND DISCUSSIONS

A. Simulation and Experimental Results

Details on investigating the performance of micro-robotics system with the use of various advanced methods of control is presented in this section. For executing and assessing the performance of various control techniques, different tests are used. For standardization, different approaches are evaluated at a particular position, i.e., for command reference, $1000 \mu\text{m}$ is used. In Fig. 12, the Simulink diagram is presented, and it exhibits different techniques of the micro robotic system. The proposed system parameters are presented in Table I, and a summary of various techniques parameters is given in Table II for the maintenance control of the micro-robotics system position at $1000 \mu\text{m}$. Table III provides the output results of the various optimization techniques in terms of time response with different objective functions, while Table IV represents comparison of the optimization techniques performance in terms of time response based on best fitness function (ISTES), while Table V describes the output result of various optimization techniques in terms of time response (Practical) based on the best fitness function (ISTES). Fig. 13, represents

the behavior by tracking the position reference with different fitness functions, while Fig. 14, represents the behavior by tracking the position reference with best fitness function. It is discovered that all practical values are higher than the simulation values for all optimization methods.

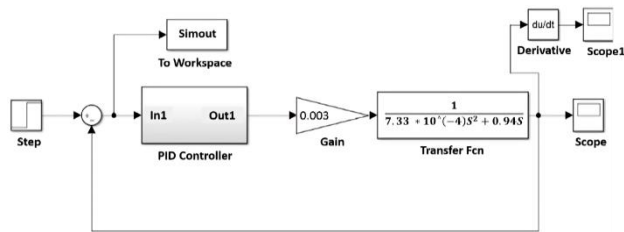


Fig. 12. Simulink diagram of the micro-robotic system with different advanced control techniques.

TABLE I. THE PROPOSED SYSTEM PARAMETERS

Name	Values	Units
Radius (r)	50	μm
Density of Water (ρ)	998.2	kgm^{-3}
Dynamic Viscosity (ζ)	1	mPa s
Mass (m)	$7.33 * 10^{-10}$	Kg
Drag Coefficient (cd)	$0.94 * 10^{-6}$	$N S m^{-1}$

TABLE II. OPTIMIZATION TECHNIQUES INPUT PARAMETERS

Optimization Techniques	Parameters	Values
All	Number of variables (nVar)	3
	Minimum value of variables (Kmin)	[0 0 0]
	Maximum value of variables (Kmax)	[100 1 1]
	Max number of iterations	25
	Number of Search Agents	30
FPA-SMA-MPA	Probability Switch	0.8

TABLE III. THE OUTPUT RESULT OF VARIOUS OPIMIZATION TECHNIQUES IN TERMS OF TIME RESPONSE WITH DIFFERENT FITNESS FUNCTIONS

Techniques	(Ideal-PID)	Control parameter			Time response	
		KP	KI	KD	t_r	t_s
FPA	IAE	100	0.55445	0	6.9262	12.0955
	ISE	100	1	0	6.9574	12.0471
	ISTES	100	0.2711	0	6.9574	12.0471
	ISTSE	100	0.6051	0	6.9312	12.0948
	ITAE	100	0.26666	0	6.8895	12.0743
	ITSE	100	1	0	6.9574	12.0471
SMA	IAE	100	0.667	0	6.9368	12.0921
	ISE	100	1	0	6.9574	12.0471
	ISTES	100	0.2672	0	6.8895	12.0744
	ISTSE	100	0.6023	0	6.9309	12.0948
	ITAE	100	0.2925	0	6.8933	12.0781
	ITSE	100	1	0	6.9574	12.0471
SSA	IAE	100	0.6669	0	6.9368	12.0921
	ISE	100	1	0	6.9574	12.0471
	ISTES	100	0.2671	0	6.8895	12.0744
	ISTSE	100	0.6048	0	6.9312	12.0948
	ITAE	100	0.2956	0	6.8938	12.0785
	ITSE	100	1	0	6.9574	12.0471
MPA	IAE	100	0.667	0	6.9368	12.0921
	ISE	100	1	0	6.9574	12.0471
	ISTES	100	0.2672	0	6.8895	12.0744
	ISTSE	100	0.6048	0	6.9312	12.0948
	ITAE	100	0.2926	0	6.8934	12.0781
	ITSE	100	1	0	6.9574	12.0471
MVO	IAE	100	0.6672	0	6.9369	12.0921
	ISE	100	1	0	6.9574	12.0471
	ISTES	100	0.2667	0	6.8895	12.0743
	ISTSE	100	0.6048	0	6.9312	12.0948
	ITAE	100	0.2918	0.0034	6.8933	12.0781
	ITSE	100	1	0	6.9574	12.0471

Table IV. COMPARISON OF THE OPTIMIZATION TECHNIQUES PERFORMANCE IN TERMS OF TIME RESPONSE BASED ON BEST FITNESS FUNCTION (ISTES).

NO	Control Technique		t_r	t_s
1	SSA	Simulation	6.8895	12.0744
		Practical	7.0294	12.0655
2	FPA	Simulation	6.8901	12.0750
		Practical	6.9950	12.8658
3	SMA	Simulation	6.8896	12.0744
		Practical	6.9944	12.8654
4	MVO	Simulation	6.8896	12.0744
		Practical	6.9944	12.8654
5	MPA	Simulation	6.8906	12.0760
		Practical	6.9955	12.8670

TABLE V. TIME RESPSES COMPARISON AMONG VARIOUS OPTIMIZATION APPROXCHES (PARACTICAL) BASED ON BEST FITNESS FUNCTION (ISTES).

No.	Control Technique	t_r	t_s	Settling error (μm)	Reduced Based on ref[3]
1	FPA	6.9950	12.8658	5.2	35%
2	SSA	7.0294	12.1655	4	50%
3	SMA	6.9944	12.8654	5.1	36.25%
4	MVO	6.9944	12.8654	5.1	36.25%
5	MPA	6.9955	12.8670	5.3	33.25%

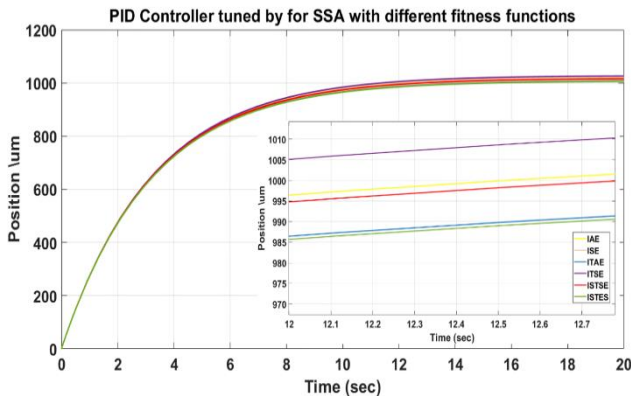


Fig. 13. Position Behavior of SSA based on PID Control with different fitness functions

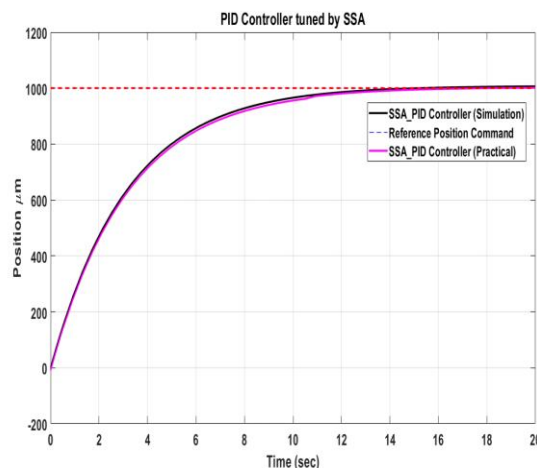


Fig. 14. Position Behavior with SSA based PID Control

B. Discussion

In this section, the five optimization techniques are thoroughly compared depending upon different fitness functions. The parameters consist of settling error and rising and settling time based on the best fitness function (ISTES). Table V exhibits the results of the measurements of FPA, SMA, MVO, MPA, and SSA which have been recorded earlier. The findings show that the settling error is reduced by 33.25%, 35%, 36.25%, 36.25%, 50% by using MPA, FPA, SMA, MVO, and SSA respectively, compared with former experiments [3]. that exhibits the highest amount of settling error It was observed that the MPA technique achieves the highest values of the rise time, settling time and settling error for both simulation and experimental results among other control approaches, while the SSA approach reduces the settling error by 50% compared to former experiments [3]. It can be concluded that the SSA technique is a promising approach for predicting real-time for the micro-robotics system.

IV. CONCLUSIONS

The paper consists of five different techniques of optimization of PID controller tuning. Based on a set of different fitness functions to discover the best performance, the ISTES achieves the highest performance. Techniques were compared on the basis of different algorithms including SSA, FPA, SMA, MPA, and MVO. It is observed that among all five, SSA outperforms all other techniques when their rising time, settling time, and settling error are compared, and thus SSA is recommended for the tuning of PID parameters based on the best fitness function (ISTES). It is observed that SSA enhances the parameter efficiency of systems by decreasing the error rate up to 50% when compared with ref [3]. For future aspects, flower pollination algorithm (FPA), sine cosine algorithm (SCA), hybrid PSO, and whale optimization algorithm (WOA) will require further investigations.

ACKNOWLEDGMENT

I would like to thanks Dr. Mohamed Sallam for his support in the experimental setup.

REFERENCES

- [1] J. Keuning. Image-based magnetic control of Microparticles, Master's thesis, University of Twente, 2011.
- [2] J. D. Keuning, J. de Vriesy, L. Abelmanny, and S. Misra, "Image-based magnetic control of paramagnetic microparticles in water," In *2011 IEEE/RSJ International Conference on Intelligent Robots and Systems*, pp. 421-426, 2011.
- [3] R. Farag, I. Badawy, F. Magdy, Z. Mahmoud, and M. Sallam, "Real-Time Trajectory Control of Potential Drug Carrier Using Pantograph "Experimental Study", " In *International Conference on Advanced Intelligent Systems and Informatics*, pp. 305-313, 2020.
- [4] J. Karl Astrom and T. Hagglund, *PID Controllers: theory, design, and tuning*, 2nd ed.: NC: Instrument Society of America, 1995.
- [5] M. Tamer, *PID Controller Implementation and Tuning*, Published by InTech, 2011.
- [6] K. Ogata, *Modern control engineering*, Prentice-Hall, 2010.
- [7] T. Häggglund and K. J. Åström. "Revisiting the Ziegler-Nichols tuning rules for PI control," *Asian J. Control*, vol. 4, no. 4, pp. 364-380, 2002.
- [8] W. Tan, J. Liu, T. Chen, and H. J. Marquez, "Comparison of some well-known PID tuning formulas," *Comput. Chem. Eng.*, vol. 39, no. 9, pp. 1416-1423, 2006.
- [9] A. Visioli, "Research trends for PID controllers," *Acta Polytech.*, vol. 52, no. 5, 2012.
- [10] D. Valériom, and J. S. Da Costa, "Tuning of fractional PID controllers with Ziegler-Nichols-type rules," *Signal Process*, vol. 86, no. 10, pp. 2771-2784, 2006.
- [11] D. K. Maghade, and B. M. Patre, "Pole placement by PID controllers to achieve time domain specifications for TITO systems," *Trans. Inst. Meas. Control.*, vol. 36, no. 4, pp. 506-522, 2014.
- [12] Z. Bingul, and O. Karahan, "Comparison of PID and FOPID controllers tuned by PSO and ABC algorithms for unstable and integrating systems with time delay," *Optim. Control Appl. Methods*, vol. 39, no. 4, 1431-1450, 2018.
- [13] D.E. Goldberg, "Genetic Algorithms in Search, Optimization, and Machine learning," 5th edition Pearson Education, 2002.
- [14] J. Kennedy, and R. Eberhart, "Particle swarm optimization," *Proc. IEEE Int. Conf. on Neural Network*, vol. 4, pp.1942 – 1948, 1995.

- [15] R. Martínez-Soto, O. Castillo, and L. T. Aguilar, "Type-1 and type-2 fuzzy logic controller design using a hybrid PSO-GA optimization method," *Inf. Sci.*, vol. 285, pp. 35-49, 2014.
- [16] M. A. Şen, V. Bakircioğlu, and M. Kalyoncu, "Performances comparison of the bees algorithm and genetic algorithm for PID controller tuning," *Proceedings of the 5th International Conference on Mechatronics and Control Engineering*, pp. 126-130, 2016.
- [17] D. T. Pham and M. Castellani, "Benchmarking and Comparison of Nature-Inspired Population-Based Continuous Optimization Algorithms," *Soft Computing - A Fusion of Foundations, Methodologies, and Applications*, vol. 18, no. 5, pp. 871-903, 2013.
- [18] P. Sharma and R. Gupta, "Tuning of PID controller for a linear BLDC motor using TLBO technique," *2014 International Conference on Computational Intelligence and Communication Networks*, pp. 1224-1228, 2014.
- [19] D. Manjarres, I. Landa-Torres, S. Gil-Lopez, J. Del Ser, M.N. Bilbao, S. Salcedo-Sanz, and Z. W. Geem, "A survey on applications of the harmony search algorithm," *Eng. Appl. Artif. Intell.*, vol. 26, no. 8, pp. 1818-1831, 2013.
- [20] Q. V. Pham, S. Mirjalili, N. Kumar, M. Alazab, and W. J. Hwang, "Whale optimization algorithm with applications to resource allocation in wireless networks," *IEEE Trans. Veh. Technol.*, vol. 69, no. 4, pp. 4285-4297, 2020.
- [21] M. Bhuyan, D. C. Das, A. K. Barik, "A comparative analysis of DSM-based autonomous hybrid microgrid using PSO and SCA," *2019 IEEE Region 10 Symposium (TENSymp)*, pp. 765-770, 2019.
- [22] M. Misaghi, and M. Yaghoobi, "Improved invasive weed optimization algorithm (IWO) based on chaos theory for the optimal design of PID controller," *J. Comput. Des. Eng.*, vol. 6, no. 3, pp. 284-295, 2019.
- [23] S. Mirjalili, S. M. Mirjalili, and A. Lewis, "Grey wolf optimizer," *Adv. Eng. Softw.*, vol. 69, pp. 46-61, 2014.
- [24] S. M. Mirjalili, S. Z. Mirjalili, S. Saremi, and S. Mirjalili, "Sine cosine algorithm: theory, literature review, and application in designing bend photonic crystal waveguides," *Nature-inspired*, pp. 201-217, 2020.
- [25] R. Pradhan, S. K. Majhi, and B. B. Pati, "Design of PID controller for automatic voltage regulator system using Ant Lion Optimizer," *World J. Eng.*, vol. 15, no. 3, pp. 373-387, 2018.
- [26] E. S. Ghith, F. A. Tolba, and S. A. Hammad, "Real-Time Implementation of Tuning PID Controller Based on Sine Cosine Algorithm for Micro-robotics System," *International Conference on Digital Technologies and Applications*, pp. 801-811, 2022.
- [27] E. S. Ghith and F. A. A. Tolba, "Real-Time Implementation of Tuning PID Controller Based on Whale Optimization Algorithm for Micro-robotics System," *2022 14th International Conference on Computer and Automation Engineering (ICCAE)*, pp. 103-109, 2022.
- [28] M. H. M. Ali, M. M. S. Mohamed, N. M. Ahmed, and M. B. A. Zahran "Comparison between P&O and SSO techniques based MPPT algorithm for photovoltaic systems," *International Journal of Electrical & Computer Engineering*, vol. 12, no. 1, pp. 32-40, 2022.
- [29] K. G. Abdullhusein, N. M. Yasin, and I. J. Hasan, "Comparison of cascade P-PI controller tuning methods for PMDC motor based on intelligence techniques," *International Journal of Electrical & Computer Engineering*, vol. 12, no. 1, pp. 1-11, 2022.
- [30] P. R. Chinda, and R. D. Rao, "A binary particle swarm optimization approach for power system security enhancement," *International Journal of Electrical & Computer Engineering*, vol. 12, no. 2, pp. 1929-1936, 2022.
- [31] M. K. Alsmadi, M. Alzaqebah, S. Jawarneh, S. Brini, I. Al-Marashdeh, K. Briki, and M. T. Al-Rashdan, "Cuckoo algorithm with great deluge local-search for feature selection problems," *International Journal of Electrical & Computer Engineering*, vol. 12, no. 4, pp. 4315-4326, 2022.
- [32] A. C. O. Reddy, and K. Madhavi, "Manta ray optimized deep contextualized bi-directional long short-term memory based adaptive galactic swarm optimization for complex question answering," *International Journal of Electrical & Computer Engineering (2088-8708)*, vol. 12, no. 4, pp. 3994-4006, 2022.
- [33] W. Aribowo, and B. S. Supari, "Optimization of PID parameters for controlling DC motor based on the aquila optimizer algorithm," *International Journal of Power Electronics and Drive Systems (IJPEDS)*, vol. 13, no. 1, pp. 808-2814, 2022.
- [34] K. J. Astrom and T. Hagglund, *PID Controllers: theory, design, and tuning*, 2nd ed.: NC: Instrument Society of America, 1995.
- [35] M. M. Eissa, G. S. Virk, A. M. AbdelGhany, E. S. Ghith, "Optimum Induction Motor Speed Control Technique using Genetic Algorithm," *American Journal of Intelligent Systems (AJIS)*, vol. 3, 2013.
- [36] M. M. Eissa, G. S. Virk, A. M. AbdelGhany, E. S. Ghith, "Optimum Induction Motor Speed Control Technique using Particle Swarm Optimization," *International Journal of Energy Engineering (IJEE)* vol. 3, no.2, March 2013, California, USA.
- [37] M. Sallam, I. Saif, Z. Saeed, and M. Fanni, "Lyapunov-based control of a teleoperation system in presence of time delay," *International Conference on Advanced Intelligent Systems and Informatics*, pp. 759-768. Springer, Cham, 2020.
- [38] X. Zhang, and D. Yuan. "A niche ant colony algorithm for parameter identification of space fractional order diffusion equation," *IAENG International Journal of Applied Mathematics*, vol. 47, no. 2, pp. 197-208, 2017.
- [39] Z. Tian, G. Wang, and Y. Ren. "AMOAIA: adaptive multi-objective optimization artificial immune algorithm," *IAENG International Journal of Applied Mathematics*, vol. 49, no. 1, pp. 1-8, 2019.
- [40] J. Wang, "A novel firefly algorithm for portfolio optimization problem," *IAENG International Journal of Applied Mathematics*, vol. 49, no. 1, pp. 1-6, 2019.
- [41] W. C. Ho, J. M. Su, and C. Y. Chang, "Maximal Market Potential of Feeder Bus Route Design Using Particle Swarm Optimization," *IAENG International Journal of Applied Mathematics*, vol. 49, no. 4, 2019.
- [42] X. Zhang, H. Huang, and X. Zhang, "Applying Cuckoo Search Algorithm to Solve Fractional Differential Equation Based on Cubic Spline Function," *IAENG International Journal of Applied Mathematics*, vol. 50, no. 1, pp. 1-12, 2020.
- [43] G. Chen, X. Zhao, Y. Xiang, X. Zeng, and H. Long, "Research on Multi-objective Active Power Optimization Simulation of Novel Improved Whale Optimization Algorithm," *IAENG International Journal of Applied Mathematics*, vol. 51, no. 3, 2021.
- [44] G. Chen, Y. Xiao, F. Long, X. Hu, and H. Long, "An Improved Marine Predators Algorithm for Short-term Hydrothermal Scheduling," *IAENG International Journal of Applied Mathematics*, vol. 51, no. 4, 2021.
- [45] C. F. Wang, and Y. H. Zhang, "An improved artificial bee colony algorithm for solving optimization problems," *IAENG International Journal of Computer Science*, vol. 43, no. 3, pp. 336-343, 2016.
- [46] G. Chen, S. Qiu, Z. Zhang, and Z. Sun, "Quasi-oppositional cuckoo search algorithm for multi-objective optimal power flow," *IAENG International Journal of Computer Science*, vol. 45, no. 2, pp. 255-266, 2018.
- [47] G. Chen, Z. Lu, Z. Zhang, and Z. Sun, "Research on hybrid modified cuckoo search algorithm for optimal reactive power dispatch problem," *IAENG International Journal of Computer Science*, vol. 45, no. 2, pp. 328-339, 2018.
- [48] B. Tutuko, S. Nurmaini, and P. S. Saparudin, "Route optimization of non-holonomic leader-follower control using dynamic particle swarm optimization," *IAENG International Journal of Computer Science*, vol. 46, no. 1, pp. 1-11, 2019.
- [49] G. Chen, J. Qian, Z. Zhang, and Z. Sun, "Multi-objective improved bat algorithm for optimizing fuel cost, emission and active power loss in power system," *IAENG International Journal of Computer Science*, vol. 46, no. 1, pp. 118-133, 2019.
- [50] S. Li, H. Liu, and Y. Du, "An Optimal Resource Allocation Scheme for Elastic Applications in Multipath Networks via Particle Swarm Optimization," *IAENG International Journal of Computer Science*, vol. 47, no. 2, 2020.
- [51] W. Z. Sun, M. Zhang, J. S. Wang, S. S. Guo, M., Wang, and W. K. Hao, "Binary Particle Swarm Optimization Algorithm Based on Z-shaped Probability Transfer Function to Solve 0-1 Knapsack Problem," *IAENG International Journal of Computer Science*, vol. 48, no. 2, 2021.
- [52] X. Shen, X. Zhang, and Z. Yu, "A New Hybrid Cuckoo Search for the Resources-Constrained Project Scheduling Problem," *IAENG International Journal of Computer Science*, vol. 48, no. 2, 2021.
- [53] A. A. Naim, and N. I. Ghali, "New Optimization Algorithm Based on Venus Flytrap Plant," *IAENG International Journal of Computer Science*, vol. 48, no. 3, 2021.
- [54] J. Yang, X. Zhang, S. Fu, and Y. Hu, "A Hybrid Harmony Search Algorithm based on Firefly Algorithm and Boltzmann Machine," *IAENG International Journal of Computer Science*, vol. 49, no. 1, 2022.
- [55] J. Xue, and B. Shen, "A novel swarm intelligence optimization approach: sparrow search algorithm," *Syst. Sci. Control Eng.*, vol. 8, no. 1, pp. 22-34, 2020.
- [56] D. Yousri, M. Abd Elaziz, and S. Mirjalili, "Fractional-order calculus-based flower pollination algorithm with local search for global optimization and image segmentation," *Knowl Based Syst.*, vol. 197,

- p. 105889, 2020.
- [57] S. Li, H. Chen, M. Wang, A. A. Heidari, and S. Mirjalili, "Slime mould algorithm: A new method for stochastic optimization," *Future Generation Computer Systems*, vol. 111, pp. 300-323, 2020.
 - [58] A. Yakout, W. Sabry, and H. M. Hasanien, "Enhancing rotor angle stability of power systems using marine predator algorithm-based cascaded PID control," *Ain Shams Eng. J.*, vol. 12, no. 2, pp. 1849-1857, 2021.
 - [59] M. A. Sobhy, A. Y. Abdelaziz, H. M. Hasanien, M. Ezzat, "Marine predators algorithm for load frequency control of modern interconnected power systems including renewable energy sources and energy storage units," *Ain Shams Eng. J.*, vol. 12, no. 4, pp. 3843-3857, 2021.
 - [60] A. Singh, and S. Suhag, "Frequency regulation in an AC microgrid interconnected with a thermal system employing multiverse-optimized fractional order-PID controller," *Int. J. Sustain. Energy*, vol. 39, no. 3, pp. 250-262, 2020.